

# The mass loss rates of OH/IR 32.8–0.3 and OH/IR 44.8–2.3

M.A.T. Groenewegen<sup>1,2</sup>

<sup>1</sup> Astronomical Institute ‘Anton Pannekoek’, Kruislaan 403, NL-1098 SJ Amsterdam, The Netherlands

<sup>2</sup> Present address: Institut d’Astrophysique de Paris, 98bis Boulevard Arago, F-75014 Paris, France

Received 2 September 1993 / Accepted 8 December 1993

**Abstract.** In a previous paper a model was presented to calculate the thermal emission of molecules around a central star. The model includes a self-consistent determination of the gas kinetic temperature, photoelectric heating, cooling by water molecules and the constraint that the presence of dust puts on the molecular excitation.

The model is applied to the CO(1–0) and CO(2–1) observations of the OH/IR stars OH 32.8–0.3 and OH 44.8–2.3 (abbreviated to OH 32.8 and OH 44.8). Both come from the sample observed by Heske et al. (1990) who noted that in the less extreme OH/IR stars (like OH 44.8) the mass loss rate derived from infrared properties agrees reasonably well with that estimated from the CO emission but that in extreme OH/IR stars (like OH 32.8) the mass loss rate derived from the infrared is an order of magnitude larger than that derived from CO emission.

For a dust opacity at 60  $\mu\text{m}$  of  $228 \text{ cm}^2 \text{ g}^{-1}$  the best model for OH 44.8 has the following parameters:  $\dot{M} = 9.0 \cdot 10^{-6} M_{\odot} \text{ yr}^{-1}$ , dust-to-gas ratio  $\Psi = 0.0035$  and mean dust grain size  $a = 0.14 \mu\text{m}$ . The derived mass loss rate is insensitive to the adopted opacity. The results are relatively insensitive to any model assumptions.

For OH 32.8 no model is found that fits the observed line profiles for a constant mass loss rate throughout the envelope. For a grain size of  $a = 0.125 \mu\text{m}$ , an opacity of  $228 \text{ cm}^2 \text{ g}^{-1}$  (following the result for OH 44.8) and a mass loss history in which the mass loss rate drops by a factor of 10 for radial distances larger than a critical distance  $R_c$ , the following model reproduces the observed intensities: (present-day)  $\dot{M} = 2.0 \cdot 10^{-5} M_{\odot} \text{ yr}^{-1}$ ,  $\Psi = 0.015$  with  $R_c \approx 1.3 \cdot 10^{17} \text{ cm}$  (corresponding to a timescale of about 2800 years). Models with  $\dot{M} \gtrsim 4.0 \cdot 10^{-5} M_{\odot} \text{ yr}^{-1}$  cannot be made to fit the observations, models with  $\dot{M} < 2.0 \cdot 10^{-5} M_{\odot} \text{ yr}^{-1}$  probably can, but result in higher dust-to-gas ratios ( $\Psi \sim \dot{M}^{-1}$ ).

The distinction made by Heske et al. (1990) between moderate OH/IR stars (like OH 44.8) and extreme OH/IR stars (like OH 32.8) can be understood as follows: the CO shell in the extreme OH/IR stars is so large that the outer part samples a previous phase of lower mass loss, several  $10^3$  yrs ago.

Finally, I comment on the possibility that in extreme mass losing stars the temperature in the outer parts of the circumstellar shells drops below the cosmic background radiation temperature. Based on the models for the two OH/IR stars I derive that this occurs if  $\dot{M}_{-5} \gtrsim 4.8 Q_{0.01} L_4^{4/3} v_{10}^{1/3}$ , where  $Q_{0.01}$  is the effective absorption coefficient in units of 0.01,  $\dot{M}_{-5}$  is the mass loss rate in  $10^{-5} M_{\odot} \text{ yr}^{-1}$ ,  $L_4$  the stellar luminosity in  $10^4 L_{\odot}$  and  $v_{10}$  the expansion velocity of the shell in  $10 \text{ km s}^{-1}$ . This relation is expected to be valid for oxygen-rich stars and standard values for the dust opacity and the photoelectric heating rate.

**Key words:** circumstellar matter – stars: individual: OH 32.8–0.3 – stars: individual: OH 44.8–2.3 – stars: AGB, post-AGB – radio lines: stars

## 1. Introduction

Heske et al. (1990) noted that the mass loss rates as derived from the infrared properties of stars and from the Knapp & Morris (1985, KM) formula for their CO emission do not agree for extreme OH/IR stars. Since it has been shown (Sahai 1990; Jura et al. 1988 (JKO); Kastner 1992) that the kinetic temperature structure can be very different from that in IRC 10 216, on which KM based their mass loss formula, a possible explanation is that the gas kinetic temperature in these stars is very different from that in IRC 10 216. Evidently, the kinetic temperature is strongly coupled to the molecular excitation.

In this paper a recent model to calculate the thermal emission of molecules in a circumstellar shell (Groenewegen 1994, Paper I) is applied to two OH/IR stars. In this model all relevant heating and cooling mechanisms are included to calculate the gas kinetic temperature in a consistent manner. The constraints that the presence of dust has on the molecular excitation is included.

In Sect. 2 the model is briefly described. In Sect. 3 a dust radiative transfer model and the molecular emission model are applied to OH 32.8–0.3 and OH 44.8–2.3. The results are discussed in Sect. 4.

Send offprint requests to: M.A.T. Groenewegen at IAP address

**Table 1.** Characteristics of OH 32.8–0.3 and OH 44.8–2.3

Star	$D$ (kpc)	$L$ ( $L_{\odot}$ )	$P$ (days)	$v_{\text{exp}}$ ( $\text{km s}^{-1}$ )	$\dot{M}$ ( $M_{\odot} \text{ yr}^{-1}$ )	$\int Tdv(1-0)$ ( $\text{K km s}^{-1}$ )	$\int Tdv(2-1)$ ( $\text{K km s}^{-1}$ )
OH 32.8–0.3	4.8	15800	1539	15.0	$1.6 \cdot 10^{-4}$	$\lesssim 4$	$14.0 \pm 0.5$
OH 44.8–2.3	1.2	3950	534	16.0	$9.0 \cdot 10^{-6}$	$13.9 \pm 0.6$	$28.5 \pm 0.6$

**Table 2.** Parameters derived from the DRT-models

Star	$\tau_5$	$r_{\text{inner}}$	$\Psi$	$Q$	$\tau_{0.1} r$ (cm) <sup>a</sup>	$T_{\text{BB}}$ (K)	$R_{\text{BB}}$ (cm)	$v_{\text{drift}}$ ( $\text{km s}^{-1}$ )
OH 32.8–0.3	4.51	8.75	0.0038	0.0136	$9.19 \cdot 10^{16}$	430	$3.0 \cdot 10^{15}$	0.64
OH 44.8–2.3	1.22	6.28	0.0070	0.0187	$8.91 \cdot 10^{15}$	815	$2.9 \cdot 10^{14}$	1.64

Note. <sup>a</sup> The optical depth at  $0.1 \mu\text{m}$  does not include scattering. The correction factors to estimate the influence of scattering are listed in Sect. 3.1.

## 2. The model

The model is explained in full detail in Paper I. Here, only the main features are outlined. The model described by Morris et al. (1985) is used to calculate the level populations. The main assumptions are spherical symmetry and the use of the Sobolev approximation (valid when the local linewidth is much smaller than the expansion velocity). The CO molecules are excited by: (1) collisions with  $\text{H}_2$  molecules, (2) interaction with the 2.8 K background radiation, and (3) infrared radiation from a central blackbody of temperature  $T_{\text{BB}}$  and radius  $R_{\text{BB}}$ . The calculations are performed using 99 gridpoints in the radial distance. Twenty-five rotational levels in the  $v = 0$  and  $v = 1$  vibrational states each are included. The line profiles are calculated at 48 velocity points.

The most important change with respect to the Morris et al. model is the inclusion of a self-consistent calculation of the kinetic temperature. The main heating processes are dust-gas collisions and the photoelectric effect on grains (in the outer part of the envelope). Heating due to cosmic rays and the temperature difference between the gas and the dust are also included in the model, but are less important. For reference, the main heating rate due to dust-gas collisions can be written as (Paper I):

$$H_{\text{dg}} = 1.2254 \cdot 10^{-40} n(\text{H}_2)^2 \frac{\Psi(1 + 4f_{\text{He}})^2}{\rho_d a} \times \left( \frac{LQv(r)}{\dot{M}} \right)^{3/2} \frac{1}{1 + \frac{v_{\text{dr}}}{v(r)}}, \quad (1)$$

with the drift velocity in  $\text{km s}^{-1}$  given by:

$$v_{\text{dr}} = 1.4293 \cdot 10^{-4} \left( \frac{LQv(r)}{\dot{M}} \right)^{0.5} \quad (2)$$

where  $\rho_d$  is the dust grain specific density in  $\text{g cm}^{-3}$ ,  $a$  the grain size in  $\mu\text{m}$ ,  $L$  the stellar luminosity in solar units,  $\dot{M}$  the mass loss rate in  $M_{\odot} \text{ yr}^{-1}$ ,  $Q$  the effective absorption coefficient (defined in Eq. 18 of Paper I),  $v(r)$  the gas velocity in  $\text{km s}^{-1}$  and  $\Psi$  the dust-to-gas ratio.

In the model adiabatic cooling is included as well as molecular cooling by  $^{12}\text{CO}$ ,  $^{13}\text{CO}$ , HCN,  $\text{H}_2$  and  $\text{H}_2\text{O}$ . Other species may be neglected. The water cooling rate is calculated from a generalization of the treatment developed by Goldreich & Scoville (1976).

The presence of dust constrains the molecular emission model. By fitting the spectral energy distribution (SED) using a dust radiative transfer (DRT) model one can determine the dust optical depth:

$$\tau_{\lambda} = 5.405 \cdot 10^8 \frac{\dot{M} \Psi Q_{\lambda} / a}{r_c R_* v_d \rho_d} \quad (3)$$

where  $\dot{M}$  is the mass loss rate in  $M_{\odot} \text{ yr}^{-1}$ ,  $v_d$  the dust velocity in  $\text{km s}^{-1}$ ,  $\Psi$  is the dust-to-gas ratio,  $Q_{\lambda}/a$  the dust absorption coefficient over de grain size in  $\text{cm}^{-1}$ ,  $\rho_d$  the grain specific density in  $\text{g cm}^{-3}$ ,  $r_c$  the inner radius in stellar radii and  $R_*$  the stellar radius in solar units. The inner radius is determined by the temperature of the dust at the inner radius,  $T_c$ . Comparing the parameters in Eq. (3) with the dominant heating rate of Eq. (1) shows that  $\dot{M}$ ,  $\Psi$ ,  $\rho_d$ ,  $a$ ,  $Q$  can not be varied independently but always must fulfill Eq. (3). JKO and Sahai (1990) also used the infrared fluxes to constrain their models, but their treatment is approximate, and only uses the far-infrared fluxes. In our model a fit to the entire SED is used.

Radiative pumping of molecules is provided by thermal emission from hot dust close to the star. In molecular models this is represented by a blackbody of temperature  $T_{\text{BB}}$  and radius  $R_{\text{BB}}$ . These quantities can be estimated from the DRT-models. At each gridpoint in the DRT-model the blackbody temperature of the radiation field is determined. In this way a realistic estimate of  $T_{\text{BB}}$  and  $R_{\text{BB}}$  is obtained. Finally, DRT-models provide  $\tau_{0.1}$  (the dust optical depth at  $0.1 \mu\text{m}$ ), which is needed to calculate the photoelectric heating rate (Eq. 10 in Paper I) and the radial dust temperature profile which is needed for the heating rate due to the gas-dust temperature difference (Eq. 7 in Paper I).

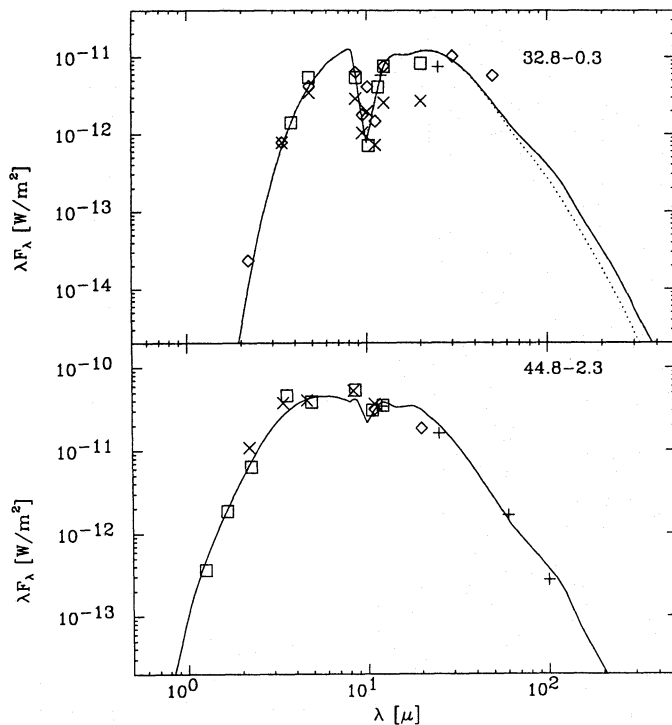


**Fig. 1.** The best-fit radiative transfer model results for OH 32.8 and OH 44.8 in the case of a constant mass loss rate (solid lines). The dotted line represents the model for OH 32.8 where the mass loss rate is a factor of 10 below the present-day value for  $r > 1.5 \cdot 10^{17}$  cm. Details are given in the text. The legend to the photometry is as follows. For OH 32.8: + = IRAS PSC, X = Evans & Beckwith (1977), ◇ = Werner et al. (1980), □ = Herman et al. (1984). For OH 44.8: + = IRAS PSC, X = Fix & Mutel (1984), ◇ = Price & Murdock (1983), □ = Ney & Merrill (1980)

### 3. OH 32.8–0.3 and OH 44.8–2.3

Heske et al. (1990) discussed two groups of OH/IR stars. Group 1 contains objects with relatively low mass loss rates ( $\dot{M} \lesssim 10^{-5} M_{\odot} \text{ yr}^{-1}$ ). The mass loss rates derived from the CO lines and other methods agree within an order of magnitude. Group 2 stars have higher mass loss rates. The mass loss rates derived from the CO lines using the KM formula are systematically lower by more than an order of magnitude compared to other methods.

From both groups one star was chosen. Criteria for selection were the availability of a phase lag distance and infrared photometry. From group 1 we selected OH 44.8–2.3, from group 2 OH 32.8–0.3. Characteristics of both stars are given in Table 1. The distances are phase lag distances as quoted by Heske et al. The uncertainty is about 0.2 kpc. The expansion velocities are averages from the OH and CO expansion velocities as quoted by Heske et al. and are accurate to within 10%. Heske et al. determined the mass loss rate using different methods. The mass loss rates quoted in Table 1 are the geometric mean values of all determinations (except the CO determination) and agree with each other within a factor of 2. These mass loss rates will be the first guess in the DRT-models and the molecular excitation calcu-

**Table 3.** OH 44.8–2.3: results of  $\chi^2$  calculations<sup>a</sup>

$a$ (in $0.05 \mu\text{m}$ ) <sup>b</sup>	$\dot{M}$ (in $10^{-6} M_{\odot} \text{ yr}^{-1}$ ) <sup>c</sup>						
	4	6	7	8	9	10	20
1	59	35	36	56	88	124	541
2	65	28	29	46	71	105	671
3	74	12	10	19	26	62	618
4	90	6.3	2.0	4.1	12	29	542
5	114	8.6	3.7	<b>0.3</b>	1.6	9.8	464
6	134	17	12	5.1	0.6	1.2	393

Notes. <sup>a</sup>  $\chi^2 \equiv \left(\frac{I(1-0)-13.9}{0.6}\right)^2 + \left(\frac{I(2-1)-28.5}{0.6}\right)^2$ , where  $I$  is the model integrated intensity.

<sup>b</sup>  $Q$  and  $a$  are varied so that  $Q/a = \text{constant}$ .

<sup>c</sup>  $\dot{M}$  and  $\Psi$  are varied so that  $\dot{M} \Psi = \text{constant}$ .

lations. For comparison, the mass loss rates based on the KM-formula for the CO lines are  $2.2 \cdot 10^{-5}$  and  $3.3 \cdot 10^{-6} M_{\odot} \text{ yr}^{-1}$  for OH 32.8 and OH 44.8, respectively (Heske et al.). The integrated intensities of the CO(1–0) and CO(2–1) lines are taken from Heske et al. as observed with the IRAM 30m telescope.

#### 3.1. The dust modelling

The dust radiative transfer model of Groenewegen (1993) is used. In this model the radiative transfer equation and the equation of thermal equilibrium are solved simultaneously for the dust. The photometric data for OH32.8 is taken from the IRAS Point Source Catalog (PSC; only 12 and 25  $\mu\text{m}$  bands available), Evans & Beckwith (1977), Werner et al. (1980) and Herman et al. (1984); for OH44.8 from the PSC (all four bands), Ney & Merrill (1980), Price & Murdock (1983) and Fix & Mutel (1984). Because both stars are highly variable (both have IRAS variability index 9) it is necessary to scale the fluxes to a common standard. Since all photometric data sets contain an observation between 10 and 13  $\mu\text{m}$ , all data sets are scaled to the IRAS 12  $\mu\text{m}$  band. The observed fluxes are corrected for interstellar extinction using Milne & Aller (1980)<sup>1</sup> and the interstellar extinction curve of Cardelli et al. (1988). The visual extinctions are 1.9 and 8.4 magnitudes for OH44.8 and OH32.8, respectively. The total flux at Earth, corrected for extinction, is  $2.2 \cdot 10^{-11}$  and  $8.9 \cdot 10^{-11} \text{ W m}^{-2}$  for OH32.8 and OH44.8. The uncertainty is about 10%. The luminosities at the assumed distances are listed in Table 1.

The following dust properties are assumed: grain radius  $a = 0.05 \mu\text{m}$ , grain density  $\rho_d = 2 \text{ g cm}^{-3}$ , condensation temperature  $T_c = 1000 \text{ K}$ . The absorption efficiency is a combination of dirty silicate (Jones & Merrill 1976) at  $\lambda < 8 \mu\text{m}$  and the silicate feature of David & Papoular (1990) at longer wavelengths. The silicate feature of David & Papoular is used for it peaks at  $10 \mu\text{m}$ , which is observed in the LRS spectra of both stars. Dirty silicate has the advantage of a high opacity in the near infrared, needed

<sup>1</sup> The visual extinction is given by  $A_V = 0.18 (1 - \exp(-11.1D(\text{kpc}) \sin(|b|))) / \sin(|b|)$

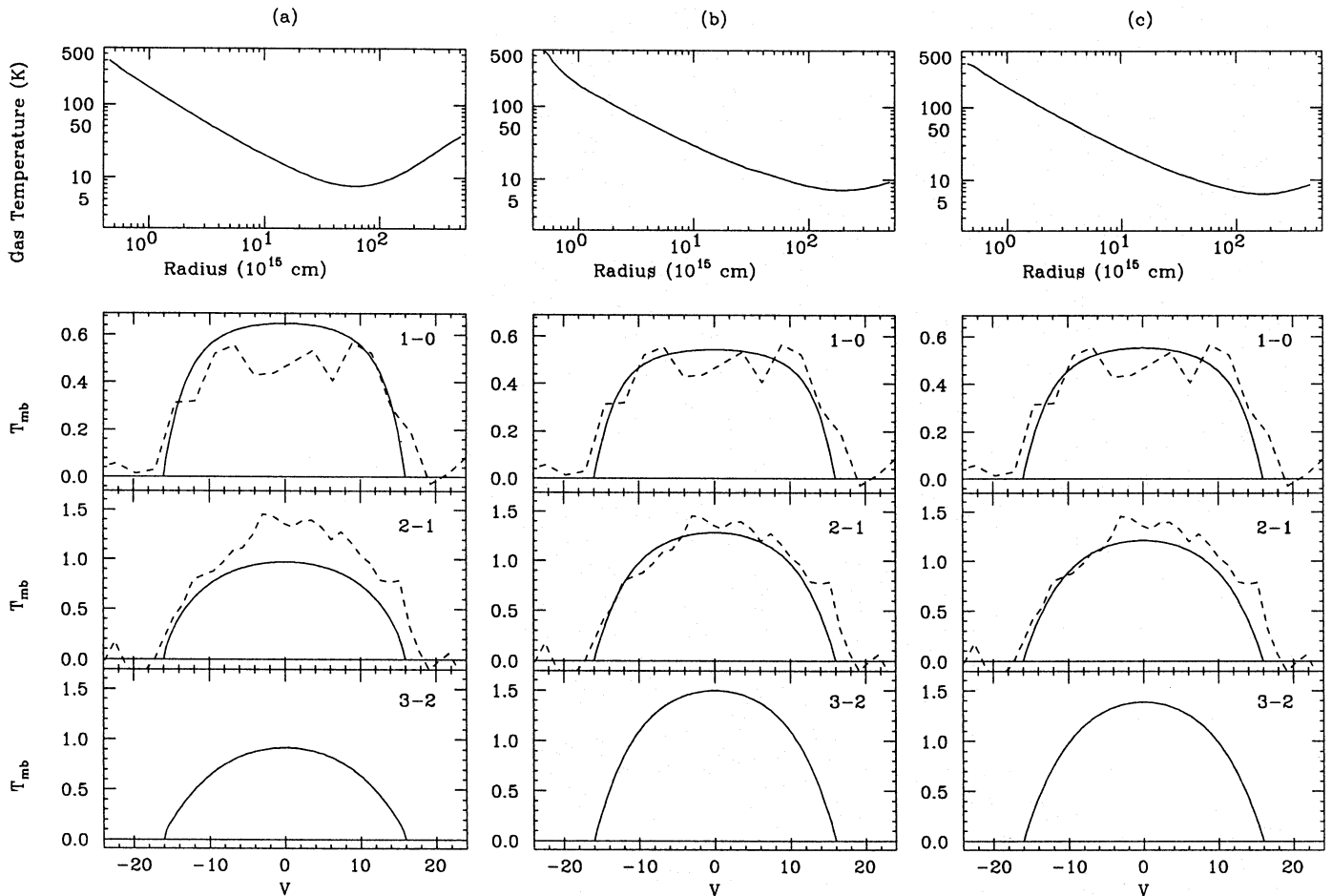


**Fig. 2a–c.** Temperature structure and line profiles for OH 44.8–2.3. **a** Model with  $\dot{M} = 9.0 \cdot 10^{-6} M_{\odot} \text{ yr}^{-1}$ ,  $\Psi = 0.0070$ ,  $Q = 0.019$ ,  $a = 0.05 \mu\text{m}$  (= standard model), **b** Model with  $\dot{M} = 8.0 \cdot 10^{-6} M_{\odot} \text{ yr}^{-1}$ ,  $\Psi = 0.0079$ ,  $Q = 0.094$ ,  $a = 0.25 \mu\text{m}$  (= best model for  $\kappa_{60} = 114 \text{ cm}^2 \text{ g}^{-1}$ ), **c** Model with  $\dot{M} = 9.0 \cdot 10^{-6} M_{\odot} \text{ yr}^{-1}$ ,  $\Psi = 0.0035$ ,  $Q = 0.105$ ,  $a = 0.14 \mu\text{m}$  (= best model for  $\kappa_{60} = 228 \text{ cm}^2 \text{ g}^{-1}$ ). The observed  $J = 1-0$  and  $2-1$  profiles (quoted rms noises 0.07 and 0.11 K, respectively) are indicated by the dotted line. The observed profiles have been shifted by the system velocity with respect to the local standard of rest as quoted in Heske et al. (1990)

to fit the spectra of oxygen-rich stars in general (Jones & Merrill 1976, Schutte & Tielens 1988). For the adopted  $Q_{\lambda}$ , the values of  $Q_{\lambda}/a$  at 1, 5, 10 and  $60 \mu\text{m}$  are 12050, 2410, 16676,  $304 \text{ cm}^{-1}$ , respectively, corresponding to opacities  $\kappa_{\lambda} = (3Q_{\lambda}/4a\rho)$  of 4520, 900, 6250,  $114 \text{ cm}^2 \text{ g}^{-1}$ , respectively.

In Fig. 1 the best fits to the spectra are shown. The optical depths at  $5 \mu\text{m}$  are 4.5 and 1.2 for OH32.8 and OH44.8, respectively, with an uncertainty of about 10%. The fit at  $\lambda > 30 \mu\text{m}$  for OH32.8 is rather poor. OH32.8 is located almost directly in the galactic plane, and contamination by cirrus is very likely. The CIRRUS-flags in the PSC catalog indicate that this is indeed the case. The PSC only lists upper limits for the IRAS 60 and  $100 \mu\text{m}$  flux-densities. Maybe the observations of Werner et al. (1980) at 30 and  $50 \mu\text{m}$  are also contaminated by cirrus.

OH44.8 has been observed at 1.3 mm by Walmsley et al. (1991). The flux they measured was  $4.8 \pm 5.6 \text{ mJy}$  (or a  $3\sigma$  upper limit of 21.6 mJy) corresponding to  $(8.5 \pm 9.9) \cdot 10^{-21} \text{ W m}^{-2} \mu\text{m}^{-1}$  (or  $< 3.8 \cdot 10^{-20} \text{ W m}^{-2} \mu\text{m}^{-1}$ ). The predicted flux at 1.3 mm is  $3.4 \cdot 10^{-21} \text{ W m}^{-2} \mu\text{m}^{-1}$ , consistent with the

upper limit. The effective temperatures of the underlying central stars can not be determined from the DRT modelling. The canonical value of 2500 K is adopted for both stars. With all other parameters in Eq. (3) known, it is then derived that the dust-to-gas ratios are 0.0038 and 0.0070 for OH32.8 and OH44.8 respectively<sup>2</sup>.

For the molecular program the optical depth at  $0.1 \mu\text{m}$ , the flux-weighted absorption efficiency and the temperature and radius of the blackbody emitting at  $4.6 \mu\text{m}$  (the wavelength of the CO  $v = (0-1)$  vibrational transition) are needed. These parameters, together with the inner radius of the dust shell (in stellar radii), the drift velocity and the dust-to-gas ratio are listed in Table 2. The extrapolation of the optical depth from 5 to  $0.1 \mu\text{m}$  assumes no scattering. An estimate of the influence of scattering may be obtained from Draine (1987) for astronomical silicate which should be indicative for our adopted  $Q_{\lambda}$  as well. The val-

<sup>2</sup> The exact choice of  $T_{\text{eff}}$  does not affect the dust-to-gas ratio. For OH32.8 it was verified that for  $T_{\text{eff}} = 2000 \text{ K}$  the dust-to-gas ratio would change to  $\Psi = 0.0036$ .

ues of  $Q_{\text{extinction}}/Q_{\text{absorption}}$  at  $0.1 \mu\text{m}$  are 1.90, 2.10, 2.21, 2.27, 2.31 and 2.35 for  $a = 0.05, 0.1, 0.15, 0.2, 0.25$  and  $0.30 \mu\text{m}$ , respectively. These are the values by which  $\tau_{0.1}$  in Table 2 has to be multiplied to estimate  $\tau_{0.1}$  including scattering.

For radii smaller than  $R_{\text{BB}}$ , I assume an undiluted blackbody of temperature  $T_{\text{BB}}(r)$ . I fitted a function of the form:

$$\log T_{\text{BB}}(r) = a + b \log(r/r_c) + c (\log(r/r_c))^2 \quad (4)$$

to the data of the DRT-modelling and find  $a = 3.081$ ,  $b = -0.735$ ,  $c = 0.557$  for OH44.8 and  $a = 3.024$ ,  $b = -0.966$ ,  $c = 0.593$  for OH32.8, respectively. The value of  $T_{\text{BB}}$  and  $R_{\text{BB}}$  listed in Table 2 correspond to the temperature and radius where the optical depth at  $4.6 \mu\text{m}$  becomes  $\sim 2/3$ .

For the dust temperature as a function of radius I fitted the same functional dependence as Eq. (4) and find  $a = 3.000$  ( $T_c = 1000 \text{ K}$  assumed for both stars),  $b = -0.678$ ,  $c = 0.076$ , and  $b = -0.696$ ,  $c = 0.063$  for OH44.8 and OH32.8 respectively.

### 3.2. The CO modelling

I first discuss the standard CO model and then comment on each star individually.

#### 3.2.1. The standard CO model

The molecular program includes all physical features of the ‘combined model’ presented in Sect. 3.11 of Paper I. The following parameters are assumed: the adiabatic index is  $\gamma = 5/3$  when  $T < 350 \text{ K}$  and  $7/5$  when  $T > 350 \text{ K}$ , helium is present with abundance  $n(\text{He})/n(\text{H}) = 0.1$ , the velocity law and drift velocity are included in the heating calculation. Heating by cosmic rays and due to the gas-dust temperature difference as well as  $\text{H}_2$  cooling are included.

No HCN is assumed to be present. Although HCN has been detected in O-rich stars the abundances are low, typically two orders of magnitude less than in carbon stars (Lindqvist et al. 1992). The CO and  $\text{H}_2\text{O}$  abundances (relative to  $\text{H}_2$ ) are set at  $f_{\text{CO}} = 6 \cdot 10^{-4}$  and  $f_{\text{H}_2\text{O}} = 1.0 \cdot 10^{-3}$ . An isotopic ratio of  $^{12}\text{CO}/^{13}\text{CO} = 25$  is assumed, in between the value measured in red giants ( $\approx 18$ , Harris et al. 1988) and non-J-type carbon stars ( $\gtrsim 30$ , Lambert et al. 1986). Water cooling is important up to  $2.4 \cdot 10^{17}$  and  $3.2 \cdot 10^{16} \text{ cm}$  in OH 32.8 and OH 44.8, respectively (Eq. 16 of Paper I).

The photoelectric effect on dust grains is included with an optical depth at  $0.1 \mu\text{m}$  including the correction factor for scattering as outlined in Sect. 3.1. Photodissociation of  $^{12}\text{CO}$  and  $^{13}\text{CO}$  is included using the formalism of Mamon et al. (1988; Eq. 19 in Paper I). From Mamon et al. (1988) it is derived that  $r_{1/2} = 1.475 \cdot 10^{18} \text{ cm}$  and  $\alpha = 3.52$  for OH 32.8 and  $r_{1/2} = 2.20 \cdot 10^{17} \text{ cm}$  and  $\alpha = 2.75$  for OH 44.8, respectively, for the standard value of the mass loss rate in Table 1. The outer radius is set at the radius where the CO abundance drops to 0.1% of the value close to the star, or  $r_{\text{outer}} = 2.8 \cdot 10^{18}$  and  $5.1 \cdot 10^{17} \text{ cm}$ , respectively.

The velocity law is taken as  $v(r) = v_{\infty}(1 - \frac{\delta}{r})^{\beta}$ , where  $v_{\infty}$  is listed in Table 1. Based on simple arguments (see e.g. Schutte

& Tielens 1989) one can estimate that  $\beta \approx 0.5$  and that the flow accelerates near the dust condensation temperature. I fixed  $\beta$  at 0.5 and determined  $\delta$  from the condition that  $v/v_{\infty} = 0.9$  at  $r = 1.5r_c$ . This results in  $\delta = 1.16 \cdot 10^{14}$  and  $4.17 \cdot 10^{13} \text{ cm}$  in OH 32.8 and OH 44.8 respectively. The precise form of the velocity law is not important because CO is collisionally excited and radiative excitation is unimportant.

Contrary to the calculations in Paper I, I did not use the CO collisional cross sections of Green & Thaddeus (1974) but the more recent ones of Fowler & Launay (1985). For transitions or temperatures not listed by them I used an extrapolation formula, using the functional dependence of formula given by the de Jong et al. (1975) and determining the coefficients  $a(\Delta j)$  and  $b(\Delta j)$  (see de Jong et al. for details) by fitting the Fowler & Launay data (1985).

#### 3.3. OH 44.8–2.3

The gas temperature profile and  $J = 1-0$ ,  $2-1$  and  $3-2$  line profiles for the standard model are shown in Fig. 2a. The integrated intensity of the  $J = 1-0$  and  $2-1$  transitions are  $16.9$  and  $23.7 \text{ K km s}^{-1}$ . The discrepancy with the observed values is at the  $5\sigma$  level. Considering the parameters involved in the heating rate (Eq. 1) and the dust optical depth (Eq. 3), the parameters  $\dot{M}$ ,  $\Psi$ ,  $Q$  and  $a$  are varied to try to obtain a better fit. Other parameters like the velocity and grain density are relatively well known and do not contribute to the uncertainty in the heating rate. To limit all possible variations of the parameters, the dust opacity is kept constant, i.e.  $Q$  and  $a$  are varied by the same factor. Consequently, since Eq. (3) enforces  $\dot{M}\Psi = \text{constant}$ , an increase in  $\dot{M}$  has to be accompanied by a similar decrease in  $\Psi$ . If  $\dot{M}$  is changed the parameters to describe the photodissociation of CO ( $r_{1/2}$  and  $\alpha$ ) and the extent to which water cooling can be important are changed accordingly. Likewise the parameter  $\tau_{0.1}$  is changed depending of the grain size (the correction for scattering). The parameter space is investigated and the result is in Table 3. The best model, shown in Fig. 2b, has the following parameters:  $\dot{M} = 8.0 \cdot 10^{-6} M_{\odot} \text{ yr}^{-1}$ ,  $\Psi = 7.8 \cdot 10^{-3}$ ,  $a = 0.25 \mu\text{m}$  and  $Q = 0.094$ . For mass loss rates in the range  $7-10 \cdot 10^{-6} M_{\odot} \text{ yr}^{-1}$  a grain size can be found which fits the observations about equally well. The dust grain sizes found are generally large,  $\gtrsim 0.20 \mu\text{m}$ , much larger than found in the interstellar medium or predicted in theoretical calculations (cf. Dominik et al. 1990).

The influence of some of the assumptions is now investigated. A major assumption is the value of the dust opacity, which is  $114 \text{ cm}^2 \text{ g}^{-1}$  at  $60 \mu\text{m}$  for the standard model (Sect. 3.1). This is lower than the values quoted by Jura (1986;  $150 \text{ cm}^2 \text{ g}^{-1}$ ) or Justtanont & Tielens (1992;  $240 \text{ cm}^2 \text{ g}^{-1}$ ). To investigate the influence of a higher opacity a new set of models was run for  $\kappa_{60} = 228 \text{ cm}^2 \text{ g}^{-1}$ . The results are collected in Table 4. The best model has  $\dot{M} = 9.0 \cdot 10^{-6} M_{\odot} \text{ yr}^{-1}$ ,  $\Psi = 3.5 \cdot 10^{-3}$ ,  $a = 0.14 \mu\text{m}$  and  $Q = 0.105$  (shown in Fig. 2c). This model is in better agreement (has a lower  $\chi^2$ ) with the observations than the best model with the lower opacity. The dust grain sizes are significantly smaller, also in better agreement with observations. The mass

**Table 4.** Additional models for OH 44.8–2.3<sup>a</sup>

$\dot{M}$ (in $10^{-6} M_{\odot} \text{ yr}^{-1}$ )	$a$ (in $0.05 \mu\text{m}$ )	$\tau_{0.1} r$ (in $8.91 \cdot 10^{15} \text{ cm}$ )	Remark	$\chi^2$
9	2.8	2.15	Best model	0.01
9	2.8	10	Influence $\tau_{0.1}$	3.5
9	2.8	0.4	Influence $\tau_{0.1}$	0.8
9	2.8	2.15	GY = 1/30	5.3
9	2.8	2.15	No water cooling	10.5

Notes. <sup>a</sup> For an opacity  $\kappa_{60} = 228 \text{ cm}^2 \text{ g}^{-1}$ .  $\dot{M}$ ,  $Q$ ,  $a$  and  $\Psi$  are varied in such a way that  $Q/a = 0.748 \mu\text{m}^{-1}$  and  $\dot{M}\Psi Q/a = \text{constant}$ .  $\chi^2$  is defined in Table 3.

loss rate is very similar to that in the low opacity case. The results are relatively insensitive to the uncertainties in the shielding of the UV radiation by dust ( $\tau_{0.1}$ ), the strength of the diffuse UV radiation field ( $G$ ) and the photoelectric yield ( $Y$ , see Eq. 10 of Paper I) or the cooling by water molecules (cf. Table 4). The line profiles in Figs. 2b, c are in good agreement with the observed ones, although both the expansion velocity and the system velocity may be slightly different from the values quoted in Heske et al. (1990).

### 3.4. OH 32.8–0.3

The gas temperature profile and line profiles for the standard model are shown in Fig. 3a. The integrated intensity of the  $J = 1-0$  and  $2-1$  lines are  $41.9$  and  $24.7 \text{ K km s}^{-1}$ , in clear discord with the observations. Remarkable is that the  $(1-0)$  intensity is larger than the  $(2-1)$  intensity. This is entirely due to the influence of photoelectric heating in the outer part of the envelope (see Sect. 4).

The parameter space in  $\dot{M}$ ,  $\Psi$ ,  $Q$  and  $a$  is investigated in a similar way as for OH 44.8 but no satisfactory model could be found. For parameter combinations for which the  $(2-1)$  intensity is near the observed value, the  $(1-0)$  intensity always remains too high. Changes in the CO or  $\text{H}_2\text{O}$  abundance, or in the dust opacity have no effect. Interstellar contamination could be a problem (cf. Heske et al. 1990) but should have affected both the  $(1-0)$  and  $(2-1)$  observations in a similar way. I am forced to conclude that one of the fundamental model assumptions (spherical symmetry and a constant mass loss rate) is incorrect. OH 32.8 has not been mapped in CO, but mapping of other oxygen-rich stars shows that the deviations from spherical symmetry are small (Bujarrabal & Alcolea 1991). OH 32.8 has been mapped in OH (Herman et al. 1985) showing that the envelope is fairly symmetric up to  $\sim 8 \cdot 10^{16} \text{ cm}$ .

To investigate a lower mass loss rate in the past, the specific case of  $Q = 0.068$  and  $a = 0.125 \mu\text{m}$  is considered, following the results for OH 44.8 ( $\kappa_{60} = 228 \text{ cm}^2 \text{ g}^{-1}$ ). Based on the observation that for some carbon-stars and oxygen-rich stars the mass loss rate seems to be related to thermal-pulses (Willems & de Jong 1988; Zijlstra et al. 1992), it is assumed that the mass loss rate is a factor  $f = 10$  below the present-day mass loss rate for distances larger than a critical distance  $R_c$ .

The models which are best in agreement with the observations are collected in Table 5 and Figs. 3b and 3c. Only models with present-day mass loss rates  $\lesssim 4.0 \cdot 10^{-5} M_{\odot} \text{ yr}^{-1}$  are in agreement with observations. Models with present-day mass loss rates  $< 2.0 \cdot 10^{-5} M_{\odot} \text{ yr}^{-1}$  probably can also be made to agree with observations but result in dust-to-gas ratios which are larger than 0.015. Table 5 shows that the result that the mass loss rate was lower in the past by a factor of  $f$  does not depend very sensitively on the assumed value of  $f$ , the opacity or the grain size. The shape of the  $(2-1)$  line profile for the  $\dot{M} = 2 \cdot 10^{-5} M_{\odot} \text{ yr}^{-1}$  model (Fig. 3c) is in somewhat better agreement with the observed one than that for the  $\dot{M} = 4 \cdot 10^{-5} M_{\odot} \text{ yr}^{-1}$  model (Fig. 3b). Figure 3 furthermore illustrates that  $J = 3-2$  observations (and also higher transitions) may be helpful in further constraining the mass loss history.

## 4. Discussion

In some of the models for OH 32.8 the integrated intensity ( $I$ ) in the  $(1-0)$  line is larger than in the  $(2-1)$  line. This is due to the photoelectric effect and an interplay of several length scales: the beam size of the telescope in the  $(1-0)$  transition at the distance of the star ( $R_{\text{beam}}$ ), the distance where photoelectric heating begins to dominate the other heating processes ( $R_{\text{UV}}$ ) and the size of the CO envelope ( $r_{1/2}$ ). The situation that  $I(1-0) > I(2-1)$  can only occur if  $R_{\text{beam}} > R_{\text{UV}}$  and  $r_{1/2} > R_{\text{UV}}$  (this is a necessary but not a sufficient condition).

The catalog of Loup et al. (1993) contains CO( $1-0$ ) and CO( $2-1$ ) data for about 125 stars. Only 5 convincing examples with  $I(1-0) > I(2-1)$  are contained in this catalog. From observations at IRAM and SEST of 22 (carbon-) stars not in Loup's catalog (or with either only the  $(1-0)$  or  $(2-1)$  transition listed; Groenewegen et al., in preparation) one additional example was discovered. So, in about 4% of the sources the two conditions derived above for  $I(1-0) > I(2-1)$  to occur are met. Of the six stars, two are carbon stars (IRAS 08074–3615, S Sct), one is a S-star (S Cas), one is a supergiant (TV Gem), one is a planetary nebula (BD 30 3069) and one is OH/IR 30.7–27.1. For S Sct (a carbon star with a detached shell) and the planetary nebula it is obvious that they have extended CO shells where photoelectric heating could indeed raise the temperature in the outer layers. The papers reporting on the CO observations were checked. The

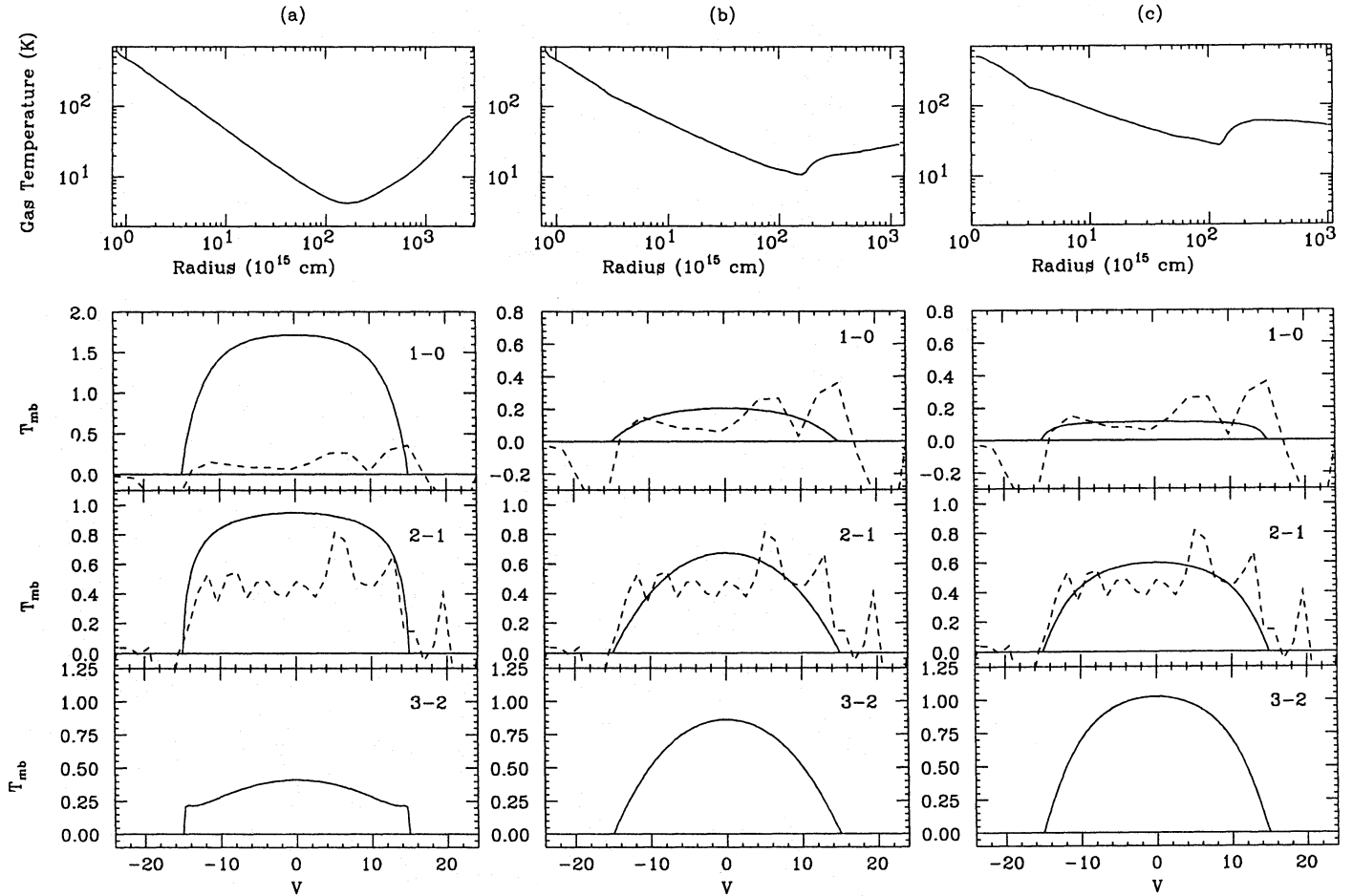


**Fig. 3a–c.** Temperature structure and line profiles for OH 32.8–0.3. **a** Model with  $\dot{M} = 1.6 \cdot 10^{-4} M_{\odot} \text{ yr}^{-1}$ ,  $\Psi = 0.0038$ ,  $Q = 0.0136$ ,  $a = 0.05 \mu\text{m}$  (= standard model), **b** Model with present-day  $\dot{M} = 4.0 \cdot 10^{-5} M_{\odot} \text{ yr}^{-1}$  and  $\dot{M} = 4.0 \cdot 10^{-6} M_{\odot} \text{ yr}^{-1}$  for  $r > 1.6 \cdot 10^{17} \text{ cm}$ ,  $\Psi = 0.0076$ ,  $Q = 0.068$ ,  $a = 0.125 \mu\text{m}$ , **c** Model with present-day  $\dot{M} = 2.0 \cdot 10^{-5} M_{\odot} \text{ yr}^{-1}$  and  $\dot{M} = 2.0 \cdot 10^{-6} M_{\odot} \text{ yr}^{-1}$  for  $r > 1.3 \cdot 10^{17} \text{ cm}$ ,  $\Psi = 0.0152$ ,  $Q = 0.068$ ,  $a = 0.125 \mu\text{m}$ . The observed  $J = 1-0$  and  $2-1$  profiles (quoted rms noises 0.05 and 0.10 K, respectively) are indicated by the dotted line. The observed profiles have been shifted by the system velocity with respect to the local standard of rest quoted in Heske et al. (1990). The upturn in the temperature structure of the gas in the top panels of **b** and **c** at  $\sim 10^{17} \text{ cm}$  is due to the mass loss history

**Table 5.** Models for OH 32.8–0.3

$\dot{M}$ ( $10^{-5} M_{\odot} \text{ yr}^{-1}$ )	$\Psi$ (in 0.0038)	$Q$ (in 0.0136)	$a$ (in $0.05 \mu\text{m}$ )	$R_c$ ( $10^{17} \text{ cm}$ )	$f$	$I(1-0)$	$I(2-1)$	$I(3-2)$
						(in $\text{K km s}^{-1}$ )		
2	4	5	2.5	1.3	10	3.1	14.0	22.9
2	4	2	1.0	1.7	10	3.9	14.0	19.4
2	8	2	2.0	1.7	10	3.9	14.0	19.4
4	2	5	2.5	1.6	10	4.5	13.9	17.8
4	2	5	2.5	1.6	100	4.3	13.7	17.7
4	2	5	2.5	1.6	5	5.1	14.3	17.9
4	2	5	2.5	1.5	5	5.0	14.0	17.7
4	4	2	2.0	2.3	10	5.9	14.0	14.5

*Note.* Columns 1, 5 and 6 are related as follows. For OH 32.8 the following mass loss history is considered. For radial distances smaller than  $R_c$ , the mass loss rate is given by the value in column 1; for distances larger than  $R_c$  the mass loss rate is a factor of  $f$  lower than the value listed in column 1.

authors only noted that the (2–1) transition is “not sufficiently excited” (Olofsson et al. 1990 for S Sct) or is “unusually low compared to (1–0)” (Heske et al. 1990 for OH 30.7), without referring to the possibility of an extra heating source in the outer most parts of the CO shell.

Related to the efficiency of the photoelectric heating rate is the question whether the gas temperature in the outer parts of circumstellar shells can drop below the cosmic background temperature, as was suggested e.g. by JKO and Sahai (1990). For OH 32.8 the temperature drops to about 4 K at  $1.8 \cdot 10^{17}$  cm in the standard model (cf. Fig. 3a). One could well imagine that the temperature drops below 2.7 K if the luminosity would have been smaller or the mass loss rate higher.

JKO showed that the thermal balance equation for the gas can be solved exactly if radiative cooling is neglected and only heating by dust-gas collisions is considered (JKO’s equation 7b). By comparing their analytic result to the calculations for OH 44.8 and OH 32.8 at  $10^{16}$  cm, I find that their relation overestimates the temperature by factors of 2.8 (OH 32.8) and 5.7 (OH 44.8). If a mean correction factor of 4.0 is assumed, then to within 50% the radius at which the gas temperature is 2.7 K is given by  $R_{2.7K} = 2.0 \cdot 10^{17} (Q_{0.01} L_4)^{1.5} (v_{10} \dot{M}_{-5})^{-0.5}$  cm, where  $Q_{0.01}$  is the effective absorption coefficient in units of 0.01,  $L_4$  the stellar luminosity in units of  $10^4 L_\odot$ ,  $v_{10}$  the expansion velocity of the shell in units of  $10 \text{ km s}^{-1}$  and  $\dot{M}_{-5}$  the mass loss rate in units of  $10^{-5} M_\odot \text{ yr}^{-1}$ . This radius is to be compared to the radius where photoelectric heating becomes important. This is expected to occur when  $\tau_{0.1} < 1$ . From Eq. (3), the results in Table 1 and the correction factor for scattering at  $0.1 \mu\text{m}$  for dust grains of  $0.05 \mu\text{m}$  I find that (for oxygen-rich stars only!) the radius at which  $\tau_{0.1} = 1$  is given by  $R_{UV} = 1.9 \cdot 10^{16} \dot{M}_{-5} / (v_{10} L_4^{0.5})$  cm. Equating  $R_{UV}$  to  $R_{2.7K}$  results in a critical mass loss rate given to within 30% by  $\dot{M}_{-5} = 4.8 Q_{0.01} L_4^{4/3} v_{10}^{1/3}$ . If for a given luminosity, effective absorption coefficient and expansion velocity the mass loss rate is higher than this critical value then gas temperatures below 2.7 K can be expected. This relation may serve as a practical guide to systematically select stars to be observed for this phenomenon.

For OH 32.8 evidence is presented for a lower mass loss rate in the past. The radius at which the mass loss rate becomes smaller is found to be  $\sim 1.5 \cdot 10^{17}$  cm, corresponding to a time scale of  $3 \cdot 10^3$  yrs. The possibility to reconstruct the mass loss history in the CO shell depends on the time interval elapsed since the mass loss rate obtained its present value (c.q. the corresponding distance  $R_c$ ), the beam size ( $R_{\text{beam}}$ ) and the extent of the CO envelope ( $r_{1/2}$ ). The mass loss history is notable in the CO emission if  $R_c < R_{\text{beam}}$  and  $R_c < r_{1/2} \sim \dot{M}^{0.6}$  (Mamon et al. 1988). This explains the segregation between the two groups of OH/IR stars discussed by Heske et al. (1990). Only the CO shells around the extreme OH/IR stars are large enough to contain information on the mass loss history.

A mass loss history does not only affect the CO emission but also the dust emission. The dotted line in Fig. 1 is the predicted SED for OH 32.8 when the mass loss rate is a factor of 10 below the present-day mass loss rate for  $r > 1.5 \cdot 10^{17}$  cm. The 100 and

$1000 \mu\text{m}$  flux-densities are reduced by factors of 1.5 and 2.3, respectively, compared to the case of a constant mass loss rate. Such differences may be observable.

The details of the mass loss history remain uncertain. In this paper a mass loss history related to thermal-pulses is adopted. Other mass loss histories probably can also fit the observations. It would be worthwhile to re-observe the sample of Heske et al. (1990) and also obtain (3–2) observations. Observations of the higher transitions would constrain the present-day mass loss rate.

If the mass loss rate were related to the phase in the thermal-pulse cycle then the present-day mass loss rate should be identified with the phase of quiescent H-burning, and the lower mass loss rate with that during the luminosity dip. The fact that apparently in most extreme OH/IR stars the mass loss rate has been lower in the past (if it is assumed that in other extreme OH/IR stars the low CO (1–0) emission is also due to a mass loss history effect) indicates that the duration of the quiescent H-burning phase can not be much longer than the  $3 \cdot 10^3$  yrs derived for OH 32.8. The interpulse period is roughly 20% longer than the duration of the quiescent H-burning phase. An interpulse period of  $5 \cdot 10^3$  yrs corresponds to a core mass of  $M_c \approx 0.9 M_\odot$  (Boothroyd & Sackmann 1988), indicating a higher than average initial mass for the progenitors of the extreme OH/IR stars. The luminosity (and indirectly the pulsation period) of OH 32.8 is consistent with this.

*Acknowledgements.* I thank Thierry Forveille for providing the observed profiles of OH 32.8 and OH 44.8 and Teije de Jong for valuable comments on the manuscript. The research of MG was supported under grant 782-373-030 by the Netherlands Foundation for Research in Astronomy (ASTRON), which is financially supported by the Netherlands Organisation for Scientific Research (NWO).

## References

- Boothroyd A.I., Sackmann I.-J., 1988, ApJ 328, 653
- Bujarrabal V., Alcolea V., 1991, A&A 251, 536
- Cardelli J.A., Clayton G.C., Mathis J.S., 1988, ApJ 345, 245
- David P., Papoular R., 1990, A&A 237, 425
- Dominik C., Gail H.-P., Sedlmayer E., Winters J.M., 1990, A&A 240, 365
- Draine B.T., 1987, Princeton Observatory Preprint 213, 1
- Evans N.J., Beckwith S., 1977, ApJ 217, 729
- Fix J.D., Mutel R.L., 1984, AJ 89, 406
- Flower D.R., Launay J.M., 1985, MNRAS 214, 271
- Goldreich P., Scoville N., 1976, ApJ 205, 144
- Green S., Thaddeus P., 1974, ApJ 191, 653
- Groenewegen M.A.T., 1994, A&A (submitted) (Paper I)
- Groenewegen M.A.T., 1993, Chapter 5, Ph.D. thesis, University of Amsterdam
- Harris M.J., Lambert D.L., Smith V.V., 1988, ApJ 325, 768
- Herman J., Baud B., Habing H.J., Winnberg A., 1985, A&A 143, 122
- Herman J., Isaacman R., Sargent A., Habing H.J., 1984, A&A 139, 71
- Heske A., Forveille T., Omont A., van der Veen W.E.C.J., Habing H.J., 1990, A&A 239, 173
- Jones T.W., Merrill K.M., 1976, ApJ 209, 509
- de Jong T., Chu S.I., Dalgarno A., 1975, ApJ 199, 69
- Jura M., 1986, ApJ 303, 327

- Jura M., Kahane C., Omont A., 1988, A&A 201, 80 (JKO)  
Justanont K., Tielens A.G.G.M., 1992, ApJ 389, 400  
Kastner J.H., 1992, ApJ 401, 337  
Knapp G.R., Morris M., 1985, ApJ 292, 640  
Lambert D.L., Gustafsson B., Eriksson K., Hinkle K.H., 1986, ApJS 62, 373  
Lindqvist M., Olofsson H., Winneberg A., Nyman L.-A., 1992, A&A 263, 183  
Loup C., Forveille T., Omont A., Paul J.F., 1993, A&AS 99, 291  
Mamon M., Glassgold A.E., Huggins P.J., 1988, ApJ 328, 797  
Milne D.K., Aller L.H., 1980, AJ 85, 17  
Morris M., Lucas R., Omont A., 1985, A&A 142, 107  
Ney E.P., Merrill K.M., 1980, The AFGL catalog, AFGL-TR-80-0050  
Olofsson H., Carlstrom U., Eriksson K., Gustafsson B., Willson, L.A., 1990, A&A 230, L13  
Price S.D., Murdock T.L., 1983, The revised AFGL catalog, AFGL-TR-83-0161  
Sahai R., 1990, ApJ 362, 652  
Schutte W.A., Tielens A.G.G.M., 1989, ApJ 343, 369  
Walmsley C.M., et al., 1991, A&A 248, 555  
Werner M.W., et al., 1980, ApJ 239, 540  
Willems F.J., de Jong T., 1988, A&A 196, 173  
Zijlstra A.A., Loup C., Waters L.B.F.M., de Jong T., 1992, A&A 265, L5